DNA Demethylation

DOI: 10.1002/anie.201406220

Pyrene-Based Quantitative Detection of the 5-Formylcytosine Loci Symmetry in the CpG Duplex Content during TET-Dependent Demethylation**

*Liang Xu, Ying-Chu Chen, Jenny Chong, Andrea Fin, Lisa S. McCoy, Jun Xu, Chao Zhang, and Dong Wang**

Abstract: *Methylcytosine (5mC) is mostly symmetrically distributed in CpG sites. Ten-eleven-translocation (TET) proteins are the key enzymes involved in active DNA demethylation through stepwise oxidation of 5mC. However, oxidation pathways of TET enzymes in the symmetrically methylated CpG context are still elusive. Employing the unique fluorescence properties of pyrene group, we designed and synthesized a sensitive fluorescence-based probe not only to target 5-formylcytosine (5fC) sites, but also to distinguish symmetric from asymmetric 5fC sites in the double stranded DNA context during TET-dependent 5mC oxidation process. Using this novel probe, we revealed dominant levels of symmetric 5fC among total 5fC sites during in vitro TET-dependent 5mC oxidation and novel mechanistic insights into the TET-dependent 5mC oxidation in the mCpG context.*

TET (ten-eleven-translocation) proteins,[1–4] the key enzymes involved in active DNA demethylation, can oxidize 5-methylcytosine (5mC) into 5-hydroxymethylcytosine (5hmC),[5,6] 5-formylcytosine (5fC),[7,8] and 5-carboxycytosine (5caC)[7,9] in a stepwise manner. These oxidized cytosine species (termed oxi-mC) are intermediates during active DNA demethylation processes.[1,4,10] TDG (thymine DNA glycosylase) can recognize and excise 5fC and/or 5caC, followed by BER (base excision repair) pathway to complete the demethylation process.[2,11–13]

[*] Dr. L. Xu, J. Chong, Dr. J. Xu, Prof. Dr. D. Wang
Skaggs School of Pharmacy and Pharmaceutical Sciences
University of California, San Diego, La Jolla, CA 92093 (USA)
E-mail: dongwang@ucsd.edu
Dr. A. Fin, Dr. L. S. McCoy
Department of Chemistry and Biochemistry
University of California, San Diego, La Jolla, CA 92093 (USA)
Y.-C. Chen, Prof. Dr. C. Zhang
Department of Chemistry, University of Southern California
Los Angeles, CA 90089 (USA)

[**] D.W. acknowledges the NIH (GM102362), Kimmel Scholar Award from the Sidney Kimmel Foundation for Cancer Research, and start-up funds from Skaggs School of Pharmacy and Pharmaceutical Sciences, UCSD for support. C.Z. acknowledges the American Cancer Society (IRG-5800754) and the University of Southern California for funding support. We appreciate Dr. Yongxuan Su and Dr. Tetsuya Kawamura (UCSD) for great help in HPLC and mass spec experiments. We appreciate Prof. Yitzhak Tor's insightful comments for this manuscript.

Supporting information for this article is available on the WWW under http://dx.doi.org/10.1002/anie.201406220.

The majority of 5mC occurs at the CpG dinucleotide motifs in a symmetric manner.[14–16] Genome-wide mapping studies also showed that the majority of oxi-mC sites are enriched in CpG islands.[17–22] Furthermore, recent structural and biochemical studies revealed that TET preferentially oxidizes 5mC in symmetric CpG sites over non-CpG sites.[23,24] While these previous studies have provided significant insights into the functional roles of oxi-mC and TET catalytic activity, several critical mechanistic questions regarding the TET oxidation process still remain unanswered, namely what the intermediates and products are of TET-dependent oxidation at the symmetrically methylated CpG (mCpG) dyads, what the distribution patterns are of oxi-mC sites in DNA duplex context, and whether there are any preferred intermediates and oxidation pathways during TET-dependent oxidation of symmetric mCpG dyads (Figure 1). Also, the question arises as to whether TET oxidize 5mC all the way to 5caC in a processive manner (TET commits consecutive

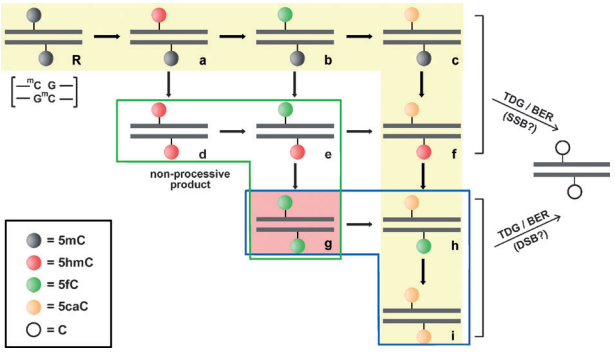

Figure 1. Potential TET oxidation products and pathways in the methylated CpG context. The possible processive pathway is highlighted in light yellow. The intermediates generated by non-processive pathways are boxed in green. The oxi-mC intermediates which may potentially generate DSB are boxed in blue. Intermediate **g** (symmetric 5fC) is the key step located in the overlap of these two boxes.

oxidation of a single 5mC site to 5 hmC, 5fC, and 5caC without disassociating from this site) or a distributive manner (TET may disassociate from DNA substrate in between each round of oxidation step).[4] However, to date, no information about oxi-mC distribution in the dsDNA context is available. The current genome-wide mapping studies did not provide enough coverage to reveal the distributions of these oxi-mC sites on CpG dyads. Furthermore, current available detection

methods of oxidized cytosines, including nuclease digestion coupled with mass spectometry or 2D-TLC analysis,[7–9,25–27] antibody-based detection,[5,21] or chemical probe detection using an aldehyde-reacting groups (such as hydroxylamine and amine),[8,20,22,28,29] are unable to provide strand-specific distribution of oxi-mC sites. It is of great urgency to develop effective methods to provide this important missing information of the oxi-mC distribution patterns in the dsDNA context (Figure 1) during TET oxidation.

Profiling the oxi-mC intermediates at the mCpG dyad of both strands would provide key mechanistic insights into TET oxidation and subsequent biological outcomes. For example, if TET consecutively oxidizes 5mC to 5hmC, 5fC, and 5caC at one site in a processive manner, we should observe only the oxi-mC intermediates highlighted in yellow (Figure 1), but not the intermediates (**d**, **e**, and **g** in Figure 1) outside of the processive route. On the other hand, if TET oxidation is carried out in a distributive manner, we should be able to detect oxi-mC intermediates **d**, **e**, and **g** (Figure 1, here we refer to as distributive-specific oxi-mC intermediates). The different oxidation intermediates and pathways could also lead to different biological outcomes. 5fC and 5caC can be excised by TDG to generate abasic sites and the strand break is induced during BER.[2,9,12] The oxi-mC intermediates **b**, **c**, **e**, and **f** (Figure 1) generate one single abasic site at a time, which typically leads to the formation of a single strand break (SSB) during TET/TDG-mediated active DNA demethylation, whereas oxi-mC intermediates **g**, **h**, and **i** (Figure 1) may generate a double strand break (DSB) during TET/TDG-mediated demethylation, which could increase the chances of introducing deleterious mutations and genome instability.[4] Finally, these distinct oxi-mC intermediates can be specifically recognized by different protein readers.[30,31]

Developing a chemical probe to quantitatively detect the oxi-mC intermediate distribution on both strands during TET oxidization is expected to uncover key insights into the TET oxidization pathways and potential outcomes (SSB and DSB) during demethylation. Here we focused on detecting the symmetric 5fC (**g**) formation, as it is one of the distributive-specific oxi-mC intermediates, which would be very informative for understanding the TET oxidation pathways. To distinguish symmetric 5fC from other asymmetric 5fC intermediates, we designed a series of chemical probes that contain a 5fC-targeting moiety as a hydrazine[32] conjugated through a linker with a pyrene fluorophore.[33] As we previously reported, the hydrazine group can selectively target 5fC through a hydrazone-based covalent bond.[32] We chose pyrene as the fluorescent reporting moiety because of its unique fluorescence signature; if the 5fC sites are located in a symmetric form of 5fCpG, the two neighboring pyrene groups of the ligand can produce distinct dimer fluorescence emission with large Stokes shift (Figure 2a).[33] Therefore, this direct targeting method can not only detect the presence of 5fC sites like previous methods but also reveal positional information of 5fC sites on both strands. Based on this strategy, we successfully detected and quantified the level of symmetric 5fC sites during in vitro TET oxidation reaction. Our results, for the first time, unveiled the preferred in vitro

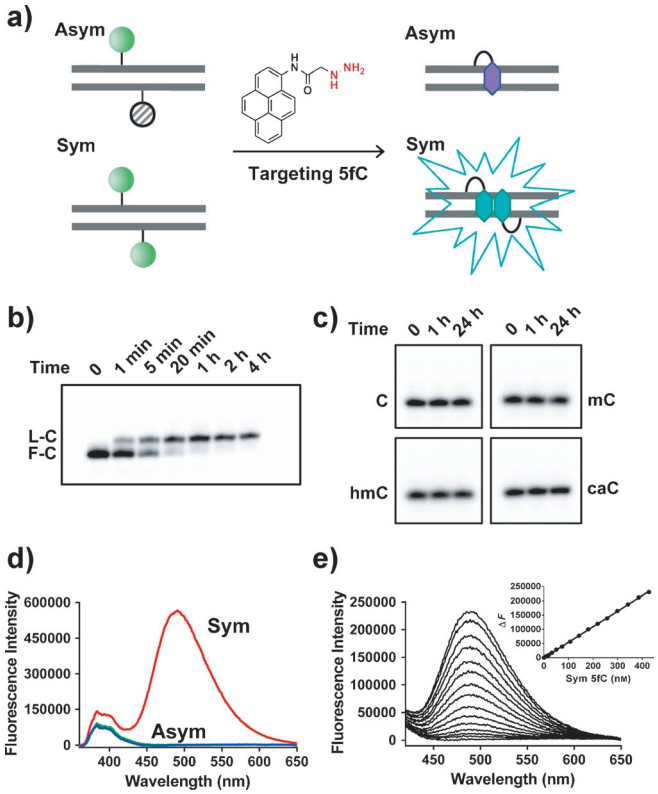

Figure 2. Pyrene–hydrazine probe as an effective chemical method to distinguish symmetric 5fCs from asymmetric 5fCs. a) Targeting 5fC by Py-Hy can generate distinct fluorescence signals between symmetric and asymmetric 5fCs. b) Gel analysis of reactivity of the Py-Hy probe with 5fC DNA. c) Gel analysis of reactivity of Py-Hy with DNA containing other forms of cytosine (C, 5mC, 5 hmC, 5caC). d) Fluorescence spectra of the Py-Hy labeling of symmetric 5fCs and asymmetric 5fCs. The fluorescence spectra of labeling of symmetric 5fC, asymmetric 5fC at top strand, and asymmetric 5fC at bottom strand are shown in red, green, and blue, respectively. e) Quantitative linear relationship between fluorescence intensity at 490 nm and the concentration of symmetric 5fC sites in the presence of 1 μM asymmetric 5fC.

TET oxidation pathways and implied potential consequences during DNA demethylation processes.

A series of compounds that conjugate a hydrazine and a pyrene group with varied linkages were designed (Supporting Information, Figure S4). These compounds are expected to form a hydrazone with the formyl group of 5fC.[32] It is reported that the linkage between pyrene and DNA has critical effect on the fluorescence excitation of the pyrene dimer.[34] Among these compounds, we chose 2-hydrazinyl-*N*-(pyren-1-yl)acetamide (Py-Hy) as the chemical probe (Scheme S1, Figures S1, S2), to target 5fC based on its strong fluorescence excitation (Figure S4), substrate specificity (Figure S5), and product stability. TLC (Figure S6), HPLC (Figure S7), and mass spectrometry analysis (Figure S8) indicated that this compound can selectively react with 5fC nucleoside through the formation of hydrazone. We further tested the reactivity and selectivity of Py-Hy ligand with synthetic 5fC-containing DNA oligos (Figures S3, S9–S11).[35] Indeed, Py-Hy can selectively target the 5fC site in DNA (F-C

DNA) and quantitatively form a covalent adduct with 5fC site (L-C DNA) in a mild environment, namely room temperature (Figure 2b; Supporting Information, Figures S9–S11). The site-specific labeling by Py-Hy of F-C DNA resulted in a defined slow-migrating single band product (L-C DNA). This conversion of L-C DNA was further verified by HPLC (Figure S10) and MALDI-TOF mass spectrometry analysis (Figure S11). In the control experiment, Py-Hy does not react with unmodified DNA oligo and DNA containing other forms of cytosines (5mC, 5hmC, 5caC; Figure 2c). Taken together, these results confirmed that Py-Hy covalently targets 5fC with high selectivity and in a quantitative manner.

To evaluate whether Py-Hy can be used to distinguish the symmetric 5fC from hemi-symmetric 5fC in the CpG context, we assembled three different DNA duplexes containing the same primary sequences. The only difference among these three DNA duplexes is the 5fC distribution pattern: one contains a fully symmetric 5fC sites, whereas the other two contain a hemi-symmetric 5fC site at either strand of duplex. After labeling with Py-Hy, we measured the fluorescent spectra of these three DNA duplexes. As shown in Figure 2d, the fluorescence spectrum for the Py-Hy labeled DNA duplex containing symmetric 5fC sites (red curve) is strikingly distinct from those of the hemi-symmetric 5fC sites (blue and black curves, weak fluorescence with short wavelength peaks around 390 nm.). The labeling of Py-Hy with symmetric 5fC site yields a new strong fluorescence signal (peak around 490 nm; circa 100 nm red-shift). In sharp contrast, there is almost no fluorescence signal at 490 nm for hemi-symmetric 5fC labeling with Py-Hy. This distinct fluorescence signature can thus be used to discriminate between two different states (symmetric and hemi-symmetric) of 5fC in the CpG dyad. To further determine whether we can quantitatively detect the signal of symmetric 5fCs in a mixture of both symmetric and asymmetric 5fCs, we tested the relationship between fluorescence intensity (490 nm) and the concentration of symmetric 5fC sites in the presence of hemi-symmetric 5fC. As shown in Figure 2e, we found that the fluorescence emission at 490 nm is in an excellent linear relationship with the abundance of symmetric 5fC sites even in the presence of high levels of asymmetric 5fCs. We can detect as low as 10 nM symmetric 5fC in the presence of 1 μM asymmetric 5fCs (100-fold excess; Figure 2e). Taken together, we can quantify the content of symmetric 5fCs by labeling a mixture of DNA with the Py-Hy probe followed by monitoring the pyrene excimer signals around 490 nm.

To investigate whether we can apply the Py-Hy probe to directly analyze 5fC states of TET oxidation products, we performed in vitro TET oxidation assays in the mCpG dyad using recombinant mTET1 catalytic domain, quenched the reaction at different time points, and then treated the oxidized products with the Py-Hy probe to label all 5fC sites. To detect and quantify the symmetric 5fC and total 5fC levels during TET oxidation, we decided to analyze the labeled products using two independent methods: quantitation of the total 5fC product level by PAGE and UV analysis, and quantification of the symmetric 5fC level by fluorescence (Figure 3a). In this way, we can calculate the percentage of symmetric 5fC sites among the total 5fC sites. This information would be helpful

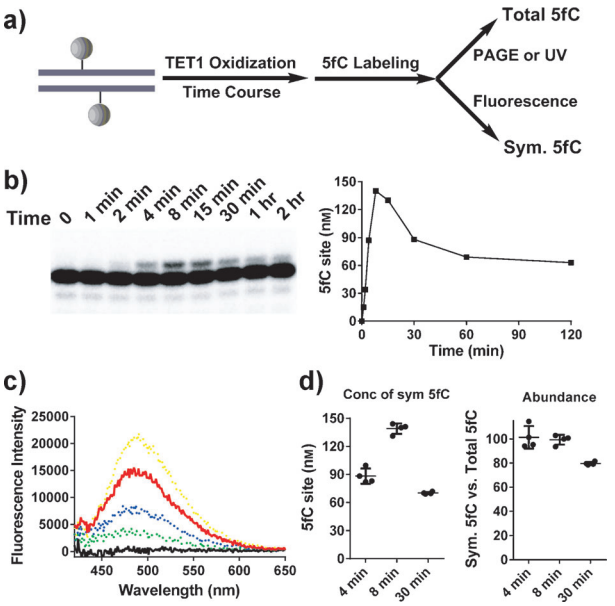

Figure 3. Detection and quantification of total and symmetric 5fC sites during in vitro TET oxidation of mCpG. a) Quantification of 5fCs during TET-dependent 5mC oxidation. b) The time-course detection (left panel) and quantification (right panel) of total 5fC generated by TET oxidation. c) Symmetric 5fC was detected by pyrene fluorescence after 8 min TET-dependent 5mC oxidation. The red curve shows the pyrene-labeled 5mC TET-oxidized product. The black curve shows the control DNA without 5mC during oxidation. The other three dashed curves refer to three mock samples with input of 50 nM (green), 100 nM (blue), and 200 nM (yellow) symmetric 5fC sites, respectively. d) Quantification of symmetric 5fC level in total 5fCs. The left panel shows the concentration of symmetric 5fCs generated by TET after 4, 8, and 30 min oxidation. The right panel shows the abundance of symmetric 5fC sites in total 5fC sites after 4, 8, and 30 min oxidation.

for us to understand whether TET oxidation of 5mC is executed through a processive or distributive mechanism and what potential biological consequences (SSB or DSB) are likely to occur after oxidation.

To monitor the total 5fC level, we performed denatured PAGE and UV absorption to analyze the labeled product at different time points during TET-dependent 5mC oxidation after confirming the 5fC generation during TET oxidation by HPLC-MS analysis of the digested oligonucleotides (Supporting Information, Figures S12 and S13). As clearly shown in Figure 3b, the total 5fC level increased at early time points and decreased with prolonged incubation time as previously observed.[7,24] Quantitative analysis (Figure 3b) indicated that the highest 5fC peak occurred at 8 min with about 14% abundance (ca. 140 nM 5fCs in 1 μM mCpGs) compared with the total cytosine species during oxidation. UV/Vis spectra further confirmed the 5fC content by measuring absorption of the conjugated pyrene group (Figure S14). To rule out the sequence effect on TET-dependent 5mC oxidation, we selected another 5mC DNA sequence for TET-dependent 5mC oxidation and found similar behavior (Figure S15).

Next, we measured the fluorescence signals of 8 min oxidation product, which has the highest total 5fC level as evidenced by gel and UV analysis. As shown in Figure 3c, we observed a significant peak at 490 nm. The presence of this

peak confirms the existence of symmetric 5fC during TET-dependent 5mC oxidation. As a control, no 490 nm signal was observed when the unmodified DNA duplex (same DNA sequence without mC sites) was treated by TET and the same labeling procedure. To further quantify the concentration of symmetric 5fC, we prepared in parallel a series of standard mixture with known concentrations of symmetric 5fC. We found a linear relationship between 5fC concentration and fluorescence intensity increase at 490 nm (Figure 3c). Based on these standard samples, we determined that circa 140 nM symmetric 5fC sites were produced from 1 μM mCpG dyads (starting material) during TET-dependent 5mC oxidation at the 8 min time point. Strikingly, the total amounts of 5fC and symmetric 5fC suggest that at the 8 min time point, almost 100% of 5fC sites generated by TET-dependent oxidation are symmetric. To further understand whether the symmetric 5fC level varied during the TET-dependent 5mC oxidation time course, we selected two additional time points either in the 5fC increasing phase (4 min) or the 5fC decreasing phase (30 min) (Figure 3d; Supporting Information, Figure S16). Fluorescence measurement and PAGE analysis showed that the symmetric 5fC level was dominant (ca. 100% of total 5fC sites) during the early phase of 5fC formation (4 min) and then decreased to about 80% of total 5fC sites after further oxidation (30 min). Furthermore, we checked the symmetric 5fC formation during TET oxidation in the context of long dsDNAs with either single or multiple methylated CpG sites to mimic the situation in genome. Similarly, we found high abundance of symmetric 5fC sites during TET oxidation in the context of all of the long dsDNA oligos we tested (either single or multiple methylated CpG sites; Supporting Information, Figures S17 and S18).

Our fluorescence results uncovered novel and unexpected mechanistic insight into the TET-dependent 5mC oxidation process. Detection of symmetric 5fCs at the CpG dyad during TET-dependent 5mC oxidation, an intermediate specific to the distributive model, suggests that the TET-dependent 5mC oxidation is not carried out in a processive manner. Rather, the TET catalytic domain most likely falls off of the binding site of nucleobase after a single round of oxidation as its cofactors (2-oxoglutarate and Fe^{II}) must be replenished to start the next oxidation cycle.[36,37] This non-processive enzymatic mode of TET-dependent oxidation may be subjected to multiple regulatory checkpoints in living cells to prevent or correct abnormal enzymatic activities.[30,38] Symmetric and unsymmetric oxi-mCpG dyads may also have different readers or distinct regulatory roles. Furthermore, the existence of symmetric 5fC sites suggests a potential consequence of generating DSB during the TET/TDG-mediated DNA demethylation pathway. How living cells prevent DSB formation and maintain genome stability during active DNA demethylation, and whether there are crosstalks between DSB repair, BER, and DNA demethylation would be interesting topics worthy of further study.

Our rationally designed chemical probe Py-Hy can distinguish the symmetric from asymmetric 5fC sites during the TET-dependent 5mC oxidation process. This chemical method also potentially allows for genome-wide profiling of symmetric and asymmetric 5fC sites. It would be interesting to determine the percentage of symmetric and asymmetric 5fC sites in vivo. Among the three isoforms of TET enzymes in mammalian cells, TET1 and TET3 contain an additional CXXC domain at the N-terminal region, which is outside of the catalytic domain compared to TET2. The CXXC domain has been found to modulate 5mC oxidation.[39] It would be interesting to test whether TET1 and TET3 produce similar distribution patterns of 5fC to TET2 during their oxidation of DNA, and whether the CXXC domain or other flanking regions outside of catalytic domain would affect the symmetric or asymmetric distribution of oxi-mC intermediates using our chemical probes in future. Furthermore, a very recent sequencing investigation found on average one strand contains lower levels of 5fC than the opposite strand across a population of cells.[40] Considering this study and our work together, it further raises the urgency to understand how the in vivo oxidation behavior of TET, and to determine the abundance and location of symmetric 5fC loci in the genome.

Our Py-Hy probe has the advantage to provide a quick and potentially high-throughput analysis of 5fC symmetry in different cell lines and cell stages to gain initial epigenetic information profiling. Furthermore, Py-Hy can also be coupled with genome-wide RNAi screening to identify novel proteins responsible for modulating symmetric/asymmetric 5fC distribution. In contrast, current genome-wide deep sequencing method is low throughput, expensive and often requires super-high coverage to reach base resolution. Therefore, these two methods can be complementary and suitable for different purposes. For example, the Py-Hy probe can be used as a pre-screening method before genome-wide deep-sequencing for comparative genome sequencing of many different cell samples. Furthermore, the fluorescence detection limit can be further improved by developing next generation fluorescent probes with increased sensitivity.

In summary, for the first time, we have developed a chemical method to quantitatively detect symmetric and asymmetric 5fC in dsDNA. Taking advantage of the unique fluorescence properties of pyrene group, our Py-Hy probe can not only specifically target 5fC but also distinguish symmetric from asymmetric 5fC sites during TET-dependent oxidation of methylated CpG context in dsDNA. Employing the pyrene-based probe, we obtained novel mechanistic insights into a previously overlooked mechanism of TET-dependent 5mC oxidation in the mCpG context. We revealed a high abundance of symmetric 5fC sites during in vitro TET-dependent 5mC oxidation, supporting a non-processive nature of the TET catalytic domain. The existence of symmetric 5fC also implies a potentially high risk of generating DSB during TET/TDG-mediated DNA demethylation. Thus, a future direction would be genome-wide profile of symmetric and asymmetric 5fC sites and their association with DSB, and development of more sensitive probes for these studies.

Received: June 13, 2014
Revised: July 21, 2014
Published online: August 27, 2014

Keywords: 5-formylcytosine · DNA demethylation · pyrene fluorescence · TET oxidation

[1] N. Bhutani, D. M. Burns, H. M. Blau, *Cell* **2011**, *146*, 866 – 872.
[2] R. M. Kohli, Y. Zhang, *Nature* **2013**, *502*, 472 – 479.
[3] W. A. Pastor, L. Aravind, A. Rao, *Nat. Rev. Mol. Cell Biol.* **2013**, *14*, 341 – 356.
[4] H. Wu, Y. Zhang, *Cell* **2014**, *156*, 45 – 68.
[5] H. Wu, Y. Zhang, *Genes Dev.* **2011**, *25*, 2436 – 2452.
[6] M. Tahiliani, K. P. Koh, Y. Shen, W. A. Pastor, H. Bandukwala, Y. Brudno, S. Agarwal, L. M. Iyer, D. R. Liu, L. Aravind, A. Rao, *Science* **2009**, *324*, 930 – 935.
[7] S. Ito, L. Shen, Q. Dai, S. C. Wu, L. B. Collins, J. A. Swenberg, C. He, Y. Zhang, *Science* **2011**, *333*, 1300 – 1303.
[8] T. Pfaffeneder, B. Hackner, M. Truss, M. Munzel, M. Muller, C. A. Deiml, C. Hagemeier, T. Carell, *Angew. Chem. Int. Ed.* **2011**, *50*, 7008 – 7012; *Angew. Chem.* **2011**, *123*, 7146 – 7150.
[9] Y. F. He, B. Z. Li, Z. Li, P. Liu, Y. Wang, Q. Tang, J. Ding, Y. Jia, Z. Chen, L. Li, Y. Sun, X. Li, Q. Dai, C. X. Song, K. Zhang, C. He, G. L. Xu, *Science* **2011**, *333*, 1303 – 1307.
[10] T. Carell, C. Brandmayr, A. Hienzsch, M. Muller, D. Pearson, V. Reiter, I. Thoma, P. Thumbs, M. Wagner, *Angew. Chem. Int. Ed.* **2012**, *51*, 7110 – 7131; *Angew. Chem.* **2012**, *124*, 7220 – 7242.
[11] A. Maiti, A. C. Drohat, *J. Biol. Chem.* **2011**, *286*, 35334 – 35338.
[12] S. R. Dalton, A. Bellacosa, *Epigenomics* **2012**, *4*, 459 – 467.
[13] L. Zhang, X. Lu, J. Lu, H. Liang, Q. Dai, G. L. Xu, C. Luo, H. Jiang, C. He, *Nat. Chem. Biol.* **2012**, *8*, 328 – 330.
[14] P. A. Jones, *Nat. Rev. Genet.* **2012**, *13*, 484 – 492.
[15] D. M. Messerschmidt, *Epigenetics* **2012**, *7*, 969 – 975.
[16] Y. Bergman, H. Cedar, *Nat. Struct. Mol. Biol.* **2013**, *20*, 274 – 281.
[17] W. A. Pastor, U. J. Pape, Y. Huang, H. R. Henderson, R. Lister, M. Ko, E. M. McLoughlin, Y. Brudno, S. Mahapatra, P. Kapranov, M. Tahiliani, G. Q. Daley, X. S. Liu, J. R. Ecker, P. M. Milos, S. Agarwal, A. Rao, *Nature* **2011**, *473*, 394 – 397.
[18] M. J. Booth, M. R. Branco, G. Ficz, D. Oxley, F. Krueger, W. Reik, S. Balasubramanian, *Science* **2012**, *336*, 934 – 937.
[19] M. Yu, G. C. Hon, K. E. Szulwach, C. X. Song, L. Zhang, A. Kim, X. Li, Q. Dai, Y. Shen, B. Park, J. H. Min, P. Jin, B. Ren, C. He, *Cell* **2012**, *149*, 1368 – 1380.
[20] E. A. Raiber, D. Beraldi, G. Ficz, H. E. Burgess, M. R. Branco, P. Murat, D. Oxley, M. J. Booth, W. Reik, S. Balasubramanian, *Genome Biol.* **2012**, *13*, R69.
[21] L. Shen, H. Wu, D. Diep, S. Yamaguchi, A. C. D'Alessio, H. L. Fung, K. Zhang, Y. Zhang, *Cell* **2013**, *153*, 692 – 706.
[22] C. X. Song, K. E. Szulwach, Q. Dai, Y. Fu, S. Q. Mao, L. Lin, C. Street, Y. Li, M. Poidevin, H. Wu, J. Gao, P. Liu, L. Li, G. L. Xu, P. Jin, C. He, *Cell* **2013**, *153*, 678 – 691.
[23] L. Hu, Z. Li, J. Cheng, Q. Rao, W. Gong, M. Liu, Y. G. Shi, J. Zhu, P. Wang, Y. Xu, *Cell* **2013**, *155*, 1545 – 1555.
[24] H. Hashimoto, J. E. Pais, X. Zhang, L. Saleh, Z. Q. Fu, N. Dai, I. R. Correa, Jr., Y. Zheng, X. Cheng, *Nature* **2014**, *506*, 391 – 395.
[25] S. Kizaki, H. Sugiyama, *Org. Biomol. Chem.* **2014**, *12*, 104 – 107.
[26] F. Samson-Thibault, G. S. Madugundu, S. Gao, J. Cadet, J. R. Wagner, *Chem. Res. Toxicol.* **2012**, *25*, 1902 – 1911.
[27] M. Münzel, D. Globisch, T. Bruckl, M. Wagner, V. Welzmiller, S. Michalakis, M. Muller, M. Biel, T. Carell, *Angew. Chem. Int. Ed.* **2010**, *49*, 5375 – 5377; *Angew. Chem.* **2010**, *122*, 5503 – 5505.
[28] P. Guo, S. Yan, J. Hu, X. Xing, C. Wang, X. Xu, X. Qiu, W. Ma, C. Lu, X. Weng, X. Zhou, *Org. Lett.* **2013**, *15*, 3266 – 3269.
[29] J. Hu, X. Xing, X. Xu, F. Wu, P. Guo, S. Yan, Z. Xu, J. Xu, X. Weng, X. Zhou, *Chem. Eur. J.* **2013**, *19*, 5836 – 5840.
[30] C. G. Spruijt, F. Gnerlich, A. H. Smits, T. Pfaffeneder, P. W. Jansen, C. Bauer, M. Munzel, M. Wagner, M. Muller, F. Khan, H. C. Eberl, A. Mensinga, A. B. Brinkman, K. Lephikov, U. Muller, J. Walter, R. Boelens, H. van Ingen, H. Leonhardt, T. Carell, M. Vermeulen, *Cell* **2013**, *152*, 1146 – 1159.
[31] M. Iurlaro, G. Ficz, D. Oxley, E. A. Raiber, M. Bachman, M. J. Booth, S. Andrews, S. Balasubramanian, W. Reik, *Genome Biol.* **2013**, *14*, R119.
[32] L. Xu, Y. C. Chen, S. Nakajima, J. Chong, L. Wang, L. Lan, C. Zhang, D. Wang, *Chem. Sci.* **2014**, *5*, 567 – 574.
[33] M. E. Østergaard, P. J. Hrdlicka, *Chem. Soc. Rev.* **2011**, *40*, 5771 – 5788.
[34] H. Mei, S. A. Ingalea, F. Seela, *Tetrahedron* **2013**, *69*, 4731 – 4742.
[35] A. S. Schröder, J. Steinbacher, B. Steigenberger, F. A. Gnerlich, S. Schiesser, T. Pfaffeneder, T. Carell, *Angew. Chem. Int. Ed.* **2014**, *53*, 315 – 318; *Angew. Chem.* **2014**, *126*, 321 – 324.
[36] K. Blaschke, K. T. Ebata, M. M. Karimi, J. A. Zepeda-Martinez, P. Goyal, S. Mahapatra, A. Tam, D. J. Laird, M. Hirst, A. Rao, M. C. Lorincz, M. Ramalho-Santos, *Nature* **2013**, *500*, 222 – 226.
[37] R. Yin, S. Q. Mao, B. Zhao, Z. Chong, Y. Yang, C. Zhao, D. Zhang, H. Huang, J. Gao, Z. Li, Y. Jiao, C. Li, S. Liu, D. Wu, W. Gu, Y. G. Yang, G. L. Xu, H. Wang, *J. Am. Chem. Soc.* **2013**, *135*, 10396 – 10403.
[38] T. Pfaffeneder, F. Spada, M. Wagner, C. Brandmayr, S. K. Laube, D. Eisen, M. Truss, J. Steinbacher, B. Hackner, O. Kotljarova, D. Schuermann, S. Michalakis, O. Kosmatchev, S. Schiesser, B. Steigenberger, N. Raddaoui, G. Kashiwazaki, U. Muller, C. G. Spruijt, M. Vermeulen, H. Leonhardt, P. Schar, M. Muller, T. Carell, *Nat. Chem. Biol.* **2014**, *10*, 574 – 581.
[39] M. Ko, J. An, H. S. Bandukwala, L. Chavez, T. Aijo, W. A. Pastor, M. F. Segal, H. Li, K. P. Koh, H. Lahdesmaki, P. G. Hogan, L. Aravind, A. Rao, *Nature* **2013**, *497*, 122 – 126.
[40] M. J. Booth, G. Marsico, M. Bachman, D. Beraldi, S. Balasubramanian, *Nat. Chem.* **2014**, *6*, 435 – 440.

